

## SUBSEQUENT NON-THERMAL EMISSION DUE TO THE KILONOVA EJECTA IN GW170817

KATSUAKI ASANO, AND SHO TO

Institute for Cosmic Ray Research, The University of Tokyo, 5-1-5 Kashiwanoha, Kashiwa, Chiba 277-8582, Japan;  
tosho@icrr.u-tokyo.ac.jp, asanok@icrr.u-tokyo.ac.jp

*Draft version November 8, 2018*

### ABSTRACT

The ejected material at the binary neutron star merger GW170817 was confirmed as a kilonova by UV, optical and IR observations. This event provides a unique opportunity to investigate the particle acceleration at a mildly relativistic shock propagating in the circum binary medium. In this paper, we simulate the non-thermal emission from electrons accelerated by the shock induced by the kilonova ejecta with a time-dependent method. The initial velocity and mass of the ejecta in the simulations are obtained from the kilonova observations in GW170817. If the ambient density is high enough ( $\geq 10^{-2} \text{ cm}^{-3}$ ), radio, optical/IR, and X-ray signals will be detected in a few years, though the off-axis short gamma-ray burst models, accounting for the X-ray/radio counterpart detected at  $\sim 10$  days after the merger, implies low ambient density. We also demonstrate that the additional low-mass ( $\sim 10^{-6} M_{\odot}$ ) component with a velocity of  $0.7\text{--}0.8c$  can reproduce the early X-ray/radio counterpart. This alternative model allows a favorably high density to detect the non-thermal emission due to the kilonova ejecta. Even for a low ambient density as  $\sim 10^{-3} \text{ cm}^{-3}$ , depending on the microscopic parameters for the electron acceleration, we can expect a growth of radio flux as  $\sim \mu\text{Jy}$  in a few years.

*Subject headings:* binaries: close — gamma-ray burst: individual (GRB 170817A) — gravitational waves — radiation mechanisms: non-thermal

### 1. INTRODUCTION

The binary neutron star merger detected as a gravitational-wave event GW170817 by the Advanced LIGO and Virgo (Abbott et al. 2017a) accompanied a weak short gamma-ray burst GRB 170817A (Abbott et al. 2017b). Furthermore, follow up observations with UV, optical and infrared telescopes found a kilonova (Arcavi et al. 2017; Cowperthwaite et al. 2017; Tanaka et al. 2017) emitted from the mildly relativistic ejecta (Lattimer & Schramm 1974; Rosswog et al. 1999; Hotokezaka et al. 2013) as expected in advance (Li & Paczyński 1998; Metzger et al. 2010; Tanaka & Hotokezaka 2013). The ejected material will form a shock propagating in the circum binary medium (CBM), and electromagnetic signals on a timescale of a few years have been predicted (Nakar & Piran 2011; Piran et al. 2013; Rosswog et al. 2013; Takami et al. 2014; Hotokezaka & Piran 2015; Hotokezaka et al. 2016). Electrons are accelerated at the shock, and emit non-thermal synchrotron photons from radio to X-ray range, which is the mildly relativistic counterpart to the emission from the supernova remnant (non-relativistic) or the gamma-ray burst (GRB) afterglow (ultra relativistic). Hereafter we call this possible phenomena “kilonova afterglow”, while the previous studies focused on mainly radio emission.

GW170817 is well localized, and its distance ( $\sim 40$  Mpc, Im et al. 2017) is exceptionally close. The physical property of the ejecta is also well constrained by the kilonova observations. Therefore, this is the golden opportunity to verify whether electrons are efficiently accelerated even in mildly relativistic case as seen in ultra relativistic shocks of GRB afterglows. In the late phase of the GRB afterglow, the shock speed may be mildly relativistic. However, the radio emission at this stage

may be dominated by the emission from the remnant electrons accelerated at the relativistic stage.

The flux of the kilonova afterglow largely depends on the CBM density  $n$ . In the context of the off-axis GRB afterglow model, the X-ray and radio counterparts of GW170817 at  $\sim 10$  days after the merger (Troja et al. 2017; Margutti et al. 2017; Alexander et al. 2017) implies a low CBM density as  $n \leq 10^{-3} \text{ cm}^{-3}$  (see also Ioka & Nakamura 2017). Such a low density leads to a very dim flux of the emission from the shocked CBM. On the other hand, alternative models for the X-ray and radio counterparts have been proposed (e.g. Kasliwal et al. 2017; Bromberg et al. 2017; Gottlieb et al. 2017; Murguia-Berthier et al. 2017). For such models, a high CBM density may be acceptable. To confirm the consistency of the off-axis GRB model also, future follow-up observations are indispensable.

In this paper, we simulate the kilonova afterglow emission from the shocked CBM with parameter sets constrained by the observations of GW170817. The evolution of the spectrum and lightcurves of radio, optical/IR, and X-ray are shown. In the most optimistic case, the radio–X-ray emission will be detected within  $\sim 1000$  days after the merger. This is also the first demonstration of the mildly relativistic calculation of our time-dependent numerical code in Fukushima et al. (2017). Another purpose of this paper is to show significant differences in the flux and its evolution between the simple analytic approximation and the numerical simulation following the evolution of the electron energy distribution.

In Section 2, we shortly review our computing method in Fukushima et al. (2017) and show model parameters. The radio, IR/optical, and X-ray lightcurves obtained from our code are shown in Section 3. Only for a high CBM density case, we can expect detections of the kilo-

nova afterglow in a few years. However, in Section 4, we demonstrate that the early X-ray and radio counterparts are explained by another shock component propagating a high CBM density. This alternative model encourages us to search for the kilonova afterglow. The conclusions are summarized in Section 5.

## 2. MODEL AND METHOD

We adopt the time-dependent numerical code developed in Fukushima et al. (2017). Our one-zone code can follow the propagation of the spherical shocked shell even for the mildly relativistic speed with the exact shock jump condition. The electron and photon energy distributions in the shell are also calculated taking into account the injection of the non-thermal electrons, radiative cooling, adiabatic cooling, synchrotron self-absorption, and photon escape. The energy and arrival time of photons escaped from the entire shell surface are consistently transformed into those for an observer with the effects of the curvature and relativistic motion of the shell.

We adopt the conventional form of the electron spectrum at the injection: the single power-law with a minimum Lorentz factor  $\gamma_m$  and high-energy exponential cutoff. Given the shock speed,  $\gamma_m$  is calculated with the exact jump condition and standard microscopic parameters for the non-thermal electrons: the energy fraction  $\epsilon_e$ , number fraction  $\eta$ , and power-law index  $p$  (see Fukushima et al. (2017) for details). The evolution of the magnetic field is obtained with the parameter  $\epsilon_B$ , which is the energy fraction of the magnetic field to the dissipated energy at the shock. The electron maximum energy is calculated considering the balance of the acceleration and radiative cooling with the acceleration time scale  $20c r_L / (3v_{\text{sh}}^2)$ , where  $v_{\text{sh}}$  is the velocity of the shock front in the CBM frame.

As shown in Fukushima et al. (2017), the exact evolutions of the shock speed and electron energy distribution lead to earlier peak time of the flux than the analytical formula. The adiabatic cooling significantly affects the electron energy distribution and resultant photon spectrum. The spectral peak flux at the cooling frequency is suppressed compared to the flux obtained with the broken power-law approximation (see also Petropoulou & Mastichiadis 2009; Pennanen et al. 2014; Uhm & Zhang 2014). The analytical approximation may be optimistic to discuss the detectability of the kilonova afterglow. To discuss the uncertainty of the parameters from observation, the comparison with the numerical results is useful.

The mass and velocity of the ejecta is constrained by the kilonova observations. Here, we refer the two component model in Cowperthwaite et al. (2017): fast component (mass  $0.01M_\odot$  and velocity  $v = 0.27c$ ) and slow component ( $0.04M_\odot$  and  $v = 0.12c$ ). The model implies the total mass of  $0.05M_\odot$  and kinetic energy of  $1.2 \times 10^{51}$  erg, which seems close to the highest value estimated in the numerical simulations (Hotokezaka et al. 2013). If the two components are distinctly decoupled, the slow ejecta will not catch up the fast ejecta before the start of its deceleration. In this case, we can neglect the contribution of the slow ejecta to the shock dynamics in early stage. Hereafter, we consider two cases: 1) only the fast ejecta is taken into account (decoupled case), and 2) the

two components are well mixed so that the average velocity is adopted as the initial velocity for the mixed single ejecta (mixed case). In the mixed case, we adopt  $0.16c$  as the initial velocity for the ejecta of  $0.05M_\odot$ .

TABLE 1  
MODEL PARAMETERS.

| Model | $n$ ( $\text{cm}^{-3}$ ) | $\eta$    | $\epsilon_B$ | Ejecta    |
|-------|--------------------------|-----------|--------------|-----------|
| A     | 0.1                      | 1         | 0.1          | Decoupled |
| A'    | 0.1                      | 1         | $10^{-3}$    | Decoupled |
| B     | $10^{-2}$                | 1         | 0.1          | Decoupled |
| B'    | $10^{-2}$                | 1         | 0.1          | Mixed     |
| C     | $10^{-3}$                | 1         | 0.1          | Decoupled |
| C'    | $10^{-3}$                | $10^{-2}$ | 0.1          | Decoupled |

Then, the remaining model parameters are the CBM density  $n$  and the microscopic parameters  $\eta$ ,  $\epsilon_e$ ,  $\epsilon_B$ , and  $p$ . Here, we fix the index  $p$  as 2.3, which is the typical value in the GRB afterglow. The parameter  $\epsilon_e$  is optimistically taken as 0.1. We summarize the parameters in Table 1 for each model. Basically, we focus on the cases of  $\eta = 1$  (all electrons are accelerated) and  $\epsilon_B = 0.1$  with the decoupled ejecta assumption, but discuss the cases changing those parameters (model name with prime mark) as well.

## 3. LIGHTCURVES

Figures 1–3 show the radio (1.4 GHz), IR (J band), and X-ray (1 keV) lightcurves, respectively. The peak time roughly corresponds to the onset of the shock deceleration. Note that after the peak time the slow ejecta may contribute to the shock dynamics for the decoupled models. In such a case, the flux decay can be shallower after the peak time. As the density decreases (see solid lines from model A to C), the peak time is delayed, and the peak flux is suppressed (Nakar & Piran 2011). The analytical formula in Piran et al. (2013) provides the peak time

$$t_{\text{peak}} = \frac{1}{v} \left( \frac{3M}{4\pi n m_p} \right)^{1/3} \quad (1)$$

$$\simeq 4.0 \times 10^3 M_{-2}^{1/3} n_{-1}^{-1/3} \beta_{0.27}^{-1} \text{ d}, \quad (2)$$

where the ejecta mass  $M = 0.01M_{-2}M_\odot$ ,  $n = 0.1n_{-1} \text{ cm}^{-3}$ , and the initial velocity  $v = 0.27\beta_{0.27}c$ . In the numerical results, the peak time slightly shifts earlier for a higher frequency. In the model A, the peak time in X-ray is  $\sim 2000$  days, while those for J band and radio are  $\sim 3000$  days and  $\sim 4000$  days, respectively. From the analytical formula, we obtain the peak flux  $\sim 14$  mJy at 1.4GHz for the model A, which is brighter than the result in Figure 1. The cooling break energy at the peak time is analytically obtained as  $\sim 0.5$  eV for the model A (Takami et al. 2014). Then, the peak fluxes are estimated as 22.4 mag at J band and  $3.5 \times 10^{-15} \text{ erg cm}^{-2} \text{ s}^{-1}$  at 1 keV, respectively.

If we seriously accept the limit on the CBM density by the off-axis GRB model (Margutti et al. 2017; Ioka & Nakamura 2017) based on the X-ray counterparts at  $\sim 10$  days after the merger, only the model C (and C') is within the allowed parameter space. However,

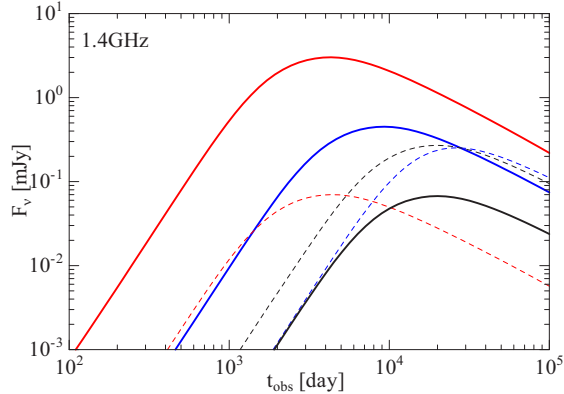


FIG. 1.— Radio (1.4GHz) lightcurves for the model A (red, solid), A' (red, dashed), B (blue, solid), B' (blue, dashed), C (black, solid), and C' (black, dashed).

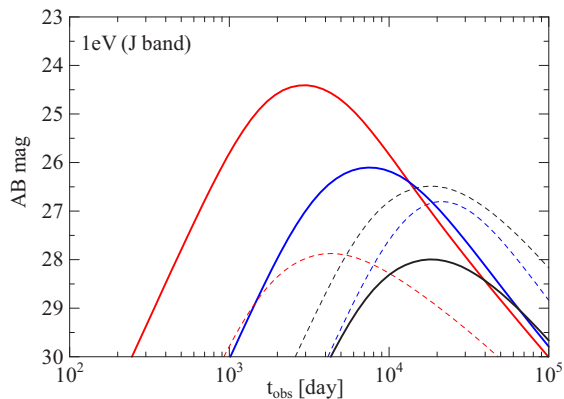


FIG. 2.— IR (1eV, J band) lightcurves for the model A (red, solid), A' (red, dashed), B (blue, solid), B' (blue, dashed), C (black, solid), and C' (black, dashed).

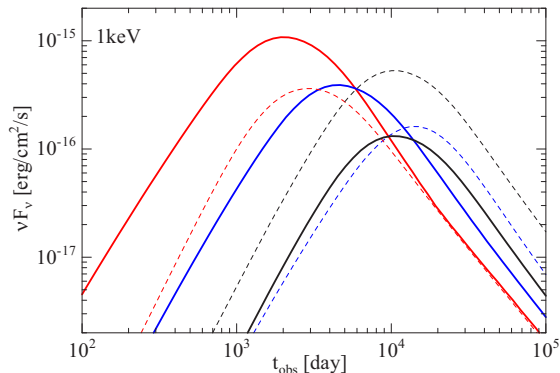


FIG. 3.— X-ray (1keV) lightcurves for the model A (red, solid), A' (red, dashed), B (blue, solid), B' (blue, dashed), C (black, solid), and C' (black, dashed).

the fluxes in the model C seems too dim to detect in a few years at any wavelength in spite of its close distance and large energy.

If the density is higher than the model constraint, the radio, IR/optical, and X-ray fluxes can be as high as current instruments can detect as shown in Figures 1–3. Especially in the most optimistic model A, the radio flux grows as  $\sim 1$  mJy at  $t \sim 10^3$  days, and  $\sim 30$   $\mu$ Jy at 1 yr. The IR/optical flux becomes brighter than 26 in AB magnitude at  $t \sim 10^3$  days. The X-ray flux also reaches the detectable level ( $\sim 10^{-15}$  erg  $\text{cm}^2$   $\text{s}^{-1}$ ) at  $t \sim 10^3$

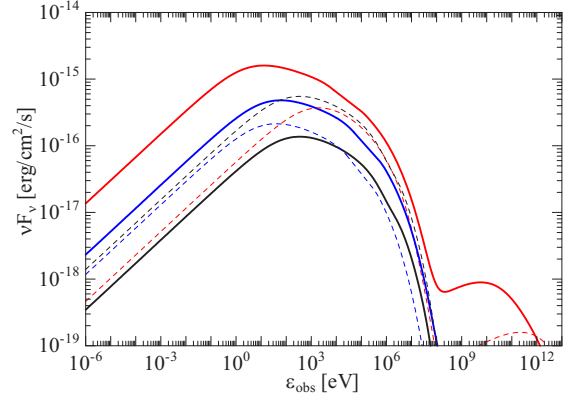


FIG. 4.— Photon spectra at the peak time of the X-ray flux for the model A (red, solid, 2,000 d), A' (red, dashed, 3,000 d), B (blue, 4700 d), B' (blue, 13,000 d), C (black, solid, 10,000 d), and C' (black, dashed, 10,000 d), respectively.

days.

A smaller value of  $\epsilon_B$  suppresses the synchrotron flux as shown in the lightcurves of the model A'. However, in the X-ray energy band, where the radiative cooling effect is significant, the flux suppression due to low  $\epsilon_B$  is not so prominent compared to those in the other bands. The X-ray peak flux in the model A' is comparable to that in the high- $\epsilon_B$  case (model A).

In the mixed ejecta case, the suppression of the initial velocity extends the peak time. As a result, the flux at the early stage is drastically suppressed (compare the model B with B' in Figures 1–3), though the total kinetic energy is larger than that in the decoupled case. The mixed ejecta is pessimistic assumption to detect the kilonova afterglow.

If the number fraction of the accelerated electrons is lower than unity, the average electron energy is boosted, which implies higher emissivity. Even for  $n = 10^{-3}$   $\text{cm}^{-3}$ , the model with  $\eta = 10^{-2}$  (model C') leads to detectable fluxes at their peak time,  $\sim 30$  yrs. Even at  $\sim 10^3$  days, the radio flux can be  $\sim \mu$ Jy for  $\eta < 1$ , which is encouraging for the follow-up observation.

The entire photon spectra at the X-ray peak time are summarized in Figure 4. In the radio band, the spectrum is consistent with  $F_\nu \propto \nu^{-(p-1)/2}$ . The peak energies correspond to the cooling frequency, which is typically in UV or X-ray band. Synchrotron self-Compton emission is expected in GeV–TeV range. However, as shown in the spectra, the flux level is far below the detection limit of the current instruments even at the X-ray peak time.

#### 4. SPHERICAL MODEL FOR THE EARLY X-RAY AND RADIO EMISSION

As shown in the previous section, the low density cases ( $n \lesssim 10^{-3}$   $\text{cm}^{-3}$ ) implied from the off-axis GRB models seem discouraging to detect the kilonova afterglow. However, the off-axis model in Murguia-Berthier et al. (2017) adopts the density of 0.3  $\text{cm}^{-3}$ . The spherical/wide-angle cocoon models by Kasliwal et al. (2017); Bromberg et al. (2017); Gottlieb et al. (2017) are alternative options to explain the low-luminosity GRB in GW170817. In such models, the early X-ray and radio emission detected at  $\sim 10$  days are not due to the decelerating relativistic jet, and the constraint for the CBM density may be relaxed. In this section, we assume another ejecta expanding spherically

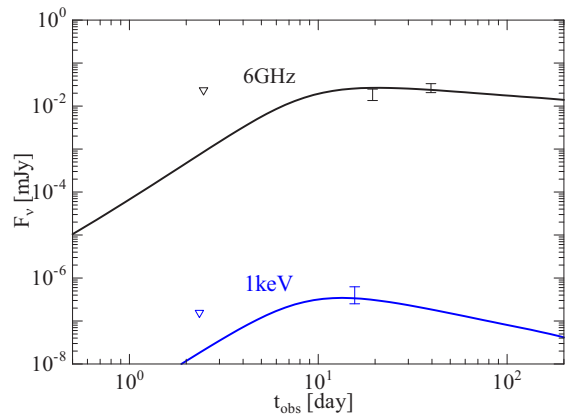


FIG. 5.— Model lightcurves for radio (6GHz, black) and X-ray (1keV, blue) in the early phase. The radio and X-ray data are taken from Alexander et al. (2017) and Margutti et al. (2017), respectively.

with a faster speed than the kilonova ejecta, and try to explain the early X-ray and radio emission for a high density case with the same numerical method.

TABLE 2

MODEL PARAMETERS FOR THE EARLY X-RAY AND RADIO EMISSION.

| Parameter        | Value                          |
|------------------|--------------------------------|
| CBM density      | $0.1 \text{ cm}^{-3}$          |
| Kinetic Energy   | $3 \times 10^{48} \text{ erg}$ |
| Ejected Mass     | $3 \times 10^{-6} M_{\odot}$   |
| Initial Velocity | $0.77c$                        |
| $\epsilon_e$     | 0.05                           |
| $\epsilon_B$     | 0.05                           |
| $\eta$           | 1                              |
| $p$              | 2.2                            |

We successfully reproduce the X-ray and radio emission with a high density of  $0.1 \text{ cm}^{-3}$  as shown in Figure 5. The model parameters are summarized in Table 2. While Murguia-Berthier et al. (2017) also tested a similar model, the initial velocity  $v = 0.77 c$  ( $\Gamma\beta = 1.2$ ) in our model is significantly slower ( $\Gamma = 5.5$  in Murguia-Berthier et al. 2017). The energy scale, mass,

and velocity are similar to those in the cocoon model of Bromberg et al. (2017) and the shock-heated ejecta in the model of Kyutoku et al. (2014). Therefore, this low-mass additional component other than the kilonova ejecta is reasonable assumption. Such a low mass component may not contribute to the kilonova emission itself, but generate the delayed emission as shown in Figure 5. In this high density scenario, the kilonova ejecta will catch up the low-mass component as it decelerates and generate the kilonova afterglow as shown in the model A in Figures 1–3.

## 5. SUMMARY

GW170817 provides a unique opportunity to verify whether electrons are efficiently accelerated even at a mildly relativistic shock. We simulate the non-thermal emission emitted from electrons accelerated at the shock propagating in the CBM. If the ambient density is higher than  $\sim 10^{-2} \text{ cm}^{-3}$ , we can expect detections of radio, optical/IR, and X-ray counterparts in a few years. If the early X-ray and radio counterparts are emitted from the shock produced by the additional low-mass ejecta of  $v \gtrsim 0.7c$ , such a high density case can be justified. In this case, the off-axis GRB model for the X-ray counterpart should be reconsidered. Even for  $n \sim 10^{-3} \text{ cm}^{-3}$ , however, optimistic parameter sets with a low  $\eta$  leads to a detectable radio flux.

On the other hand, Murase et al. (2017) proposed another type of the delayed electromagnetic counterparts due to the long-lasting activity of the central objects, such as the disk-driven outflows or pulsar winds. The emission timescale in the long-lasting engine model is shorter; typically the flux peaks in a year, differently from the case in the kilonova ejecta model. Future follow-up observations are important to verify such various possibilities.

This work is supported by the joint research program of the Institute for Cosmic Ray Research (ICRR), The University of Tokyo, and Grants-in-Aid for Scientific Research nos. 15K05069, 16K05291 (K.A.) from the Ministry of Education, Culture, Sports, Science and Technology (MEXT) of Japan. We also appreciate S. Kisaka for his useful comment.

## REFERENCES

- Abbott, B. P., Abbott, R., Abbott, T. D., et al., 2017, Phys. Rev. Lett., 119, 161101
- Abbott, B. P., Abbott, R., Abbott, T. D., et al., 2017, ApJ, 848, L13
- Alexander, K. D., Berger, E., Fong, W., et al., 2017, ApJ, 848, L21
- Arcavi, I., Hosseinzadeh, G., Howell, D. A., et al., 2017, Nature, 551, 64
- Bromberg, O., Tchekhovskoy, A., Gottlieb, O., Nakar, E., & Piran, T., 2017, arXiv:1710.05897
- Cowperthwaite, P. S., Berger, E., Villar, V. A., et al., 2017, ApJ, 848, L17
- Fukushima, T., To, S., Asano, K., & Fujita, Y., 2017, ApJ, 844, 92
- Gottlieb, O., Nakar, E., Piran, T., & Hotokezaka, K., 2017, arXiv:1710.05896
- Hotokezaka, K., Kiuchi, K., Kyutoku, K., et al., 2013, Phys. Rev. D, 87, 024001
- Hotokezaka, K., Nissanke, S., Hallinan, G., et al., 2016, ApJ, 831, 190
- Hotokezaka, K., & Piran, T., 2015, MNRAS, 450, 1430
- Im, M., Yoon, Y., Lee, S.-K. J., et al., 2017, ApJ, 849, L16
- Ioka, K., & Nakamura, T., 2017, arXiv:1710.05905
- Kasliwal, M. M., Nakar, E., Singer, L. P., et al., 2017, Sci, 10.1126/science.aap9455
- Kyutoku, K., Ioka, K., & Shibata, M., 2014, MNRAS, 437, L6
- Lattimer, J. M., & Schramm, D. N., 1974, ApJ, 192, L145
- Li, L.-X., & Paczyński, B., 1998, ApJ507, L59
- Margutti, R., Berger, E., Fong, W., et al., 2017, ApJ, 848, L20
- Metzger, B. D., Martínez-Pinedo, G., Darbha, S., et al., 2010, MNRAS, 406, 2650
- Murguia-Berthier, A., Ramirez-Ruiz, E., Kilpatrick, C. D., et al., 2017, ApJ, 848, L34
- Murase, K., Toomey, M. W., Fang, K., et al., 2017, arXiv:1710.10757
- Nakar, E., & Piran, T., 2011, Nature, 478, 82
- Pennanen, T., Vurm, I., & Poutanen, J. 2014, A&A, 564, A77
- Petropoulou, M., & Mastichiadis A. 2009, A&A, 507, 599
- Piran, T., Nakar, E., & Rosswog, S., 2013, MNRAS, 430, 2121
- Rosswog, S., Liebendörfer, M., Thielemann, F.-K., Davies, M. B., Benz, W., & Piran, T., 1999, A&A, 341, 499

Rosswog, S., Piran, T., & Nakar, E., 2013, MNRAS, 430, 2585  
Takami, H., Kyutoku, K., & Ioka, K., 2014, Phys. Rev. D, 89,  
063006  
Tanaka, M., & Hotokezaka, K., 2013, ApJ, 775, 113

Tanaka, M., Utsumi, Y., Mazzali, P. A., et al., 2017, PASJ,  
psx121  
Troja, E., Piro, L., van Eerten, H., et al., 2017, Nature, 551, 71  
Uhm, Z. L., & Zhang, B. 2014, ApJ, 780, 82